Provided for non-commercial research and education use.
Not for reproduction, distribution or commercial use.

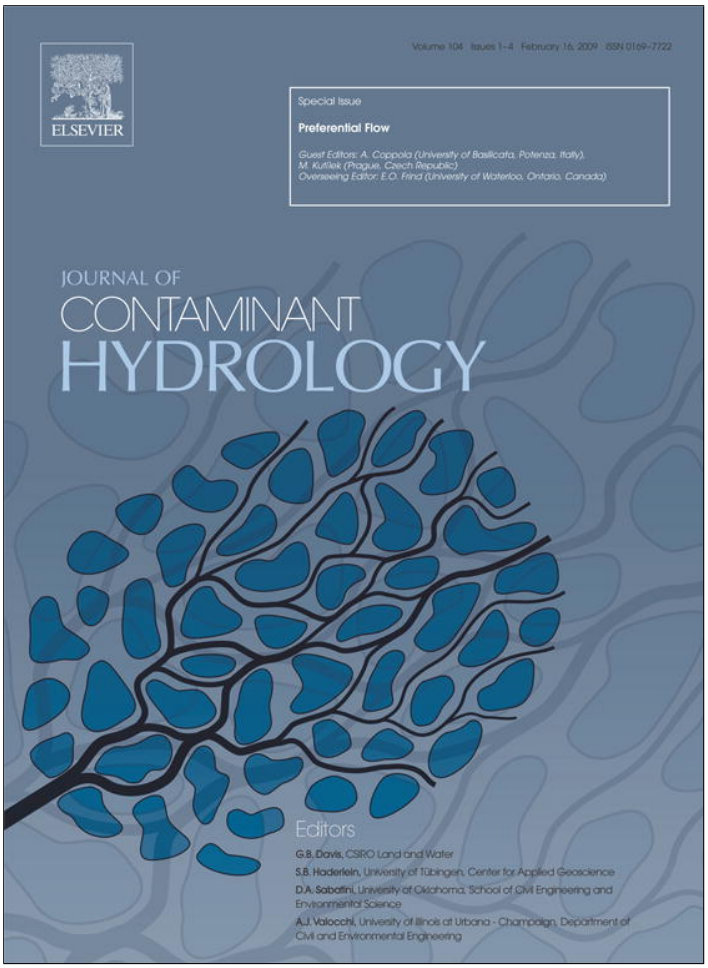

This article appeared in a journal published by Elsevier. The attached copy is furnished to the author for internal non-commercial research and education use, including for instruction at the authors institution and sharing with colleagues.

Other uses, including reproduction and distribution, or selling or licensing copies, or posting to personal, institutional or third party websites are prohibited.

In most cases authors are permitted to post their version of the article (e.g. in Word or Tex form) to their personal website or institutional repository. Authors requiring further information regarding Elsevier's archiving and manuscript policies are encouraged to visit:

http://www.elsevier.com/copyright

Author's personal copy

Journal of Contaminant Hydrology 104 (2009) 107–125

Contents lists available at ScienceDirect

Journal of Contaminant Hydrology

journal homepage: www.elsevier.com/locate/jconhyd

Impact of varying soil structure on transport processes in different diagnostic horizons of three soil types

Radka Kodešová [a,*], Nadia Vignozzi [b], Marcela Rohošková [a], Tereza Hájková [a], Martin Kočárek [a], Marcello Pagliai [b], Josef Kozák [a], Jirka Šimůnek [c]

[a] Dept. of Soil Science and Soil Protection, Czech University of Life Sciences Prague, Kamýcká 129, 16521 Prague 6, Czech Republic
[b] CRA-ABP, Centro di ricerca per l'agrobiologia e la pedologia, Piazza M Azeglio 30, I-50121 Florence, Italy
[c] Dept. of Environmental Sciences, University of California Riverside, 900 University Avenue, Riverside, CA 92521, USA

ARTICLE INFO

Article history:
Received 12 April 2008
Received in revised form 13 October 2008
Accepted 22 October 2008
Available online 31 October 2008

Keywords:
Soil pore structure
Soil structure stability
Column experiment
Preferential flow
Pesticide transport
Single-porosity model
Dual-permeability model
Two-site sorption model

ABSTRACT

When soil structure varies in different soil types and the horizons of these soil types, it has a significant impact on water flow and contaminant transport in soils. This paper focuses on the effect of soil structure variations on the transport of pesticides in the soil above the water table. Transport of a pesticide (chlorotoluron) initially applied on soil columns taken from various horizons of three different soil types (Haplic Luvisol, Greyic Phaeozem and Haplic Cambisol) was studied using two scenarios of ponding infiltration. The highest infiltration rate and pesticide mobility were observed for the Bt_1 horizon of Haplic Luvisol that exhibited a well-developed prismatic structure. The lowest infiltration rate was measured for the Bw horizon of Haplic Cambisol, which had a poorly developed soil structure and a low fraction of large capillary pores and gravitational pores. Water infiltration rates were reduced during the experiments by a soil structure breakdown, swelling of clay and/or air entrapped in soil samples. The largest soil structure breakdown and infiltration decrease was observed for the Ap horizon of Haplic Luvisol due to the low aggregate stability of the initially well-aggregated soil. Single-porosity and dual-permeability (with matrix and macropore domains) flow models in HYDRUS-1D were used to estimate soil hydraulic parameters via numerical inversion using data from the first infiltration experiment. A fraction of the macropore domain in the dual-permeability model was estimated using the micro-morphological images. Final soil hydraulic parameters determined using the single-porosity and dual-permeability models were subsequently used to optimize solute transport parameters. To improve numerical inversion results, the two-site sorption model was also applied. Although structural changes observed during the experiment affected water flow and solute transport, the dual-permeability model together with the two-site sorption model proved to be able to approximate experimental data.
© 2008 Elsevier B.V. All rights reserved.

1. Introduction

Soil and groundwater contamination caused by pesticides used in agriculture is an environmental problem worldwide. The controlling processes, which include water flow and contaminant transport, strongly depend on the composition of soil structure components resulting from pedogenesis and soil management. Different compositions of soil structure components are reflected in soil properties that affect water and solute transport, such as the soil structure and the configuration of the soil porous system, the aggregate stability, and soil hydraulic properties. Soil aggregation is under the control of different mechanisms in different soil types. Flocculated clay particles, or their complexes with humus (organo-mineral complexes) and soil organic matter, act as the main cementing agents in soil aggregates. The cementing effect of free Fe and Al oxides is important in soils with low organic matter content (Six et al., 2002). Generally, the level of aggregation and the stability of aggregates increase with

* Corresponding author.
E-mail address: kodesova@af.czu.cz (R. Kodešová).

0169-7722/$ – see front matter © 2008 Elsevier B.V. All rights reserved.
doi:10.1016/j.jconhyd.2008.10.008

Author's personal copy

increasing organic matter content, surface area of clay minerals, and cation exchange capacity (Bronick and Lal, 2005). In addition to soil properties, soil management also has a very important influence on the stability of soil structure. By tillage the topsoil is mixed and new aggregates are exposed to different breakdown mechanisms (Six et al., 1998). Soil processing at improper soil moisture, crossing of heavy machinery, irrigation, and use of fertilizers can also lead to soil structure degradation (Pagliai et al., 2003, 2004 and Servadio et al., 2005). Soil structure, soil porous systems and subsequently soil hydraulic properties are also influenced by many additional factors, including the mineralogical composition of the parent material, its alteration degree, organic matter content, soil water regime, transport processes within the soil profile, climate, plant roots, soil organisms, and management practices.

The shapes and sizes of soil pores can be studied by image analysis of thin soil sections at various magnifications. Porous systems with macropores and their impact on saturated hydraulic conductivities, K_s, were explored by Bouma et al. (1977, 1979) using micromorphometric data. Differently shaped pores in soils under different management practices and their K_s values were studied by Pagliai et al. (1983, 2003, 2004) using both micromorphometric and micromorphological investigations. Finally, Kodešová et al. (2006, 2007, 2008) described the effects of gravitational pores and large capillary pores detectable in micromorphometric images on the shape of soil hydraulics functions.

Multi-modality of the soil porous system and hierarchical pore composition may cause non-equilibrium water flow and solute transport in soils. Numerical models that assume multi-modal soil porous systems have been developed to describe non-equilibrium water flow and solute transport in such soils. Overviews of various approaches were given by Šimůnek et al. (2003), Gerke (2006), Köhne et al. (2009a,b-this issue), or Šimůnek and van Genuchten (2008b). In these models the soil porous system is divided into two domains, and each domain is characterized by its own set of transport properties and equations describing flow and transport processes. The dual-porosity approach defines water flow and solute transport in systems consisting of domains of both mobile and immobile water. The dual-porosity formulation is based on a set of equations describing water flow and solute transport in the mobile domain, and mass balance equations describing soil water and solute content in the immobile domain. On the other hand, the dual-permeability approach assumes that water flow and solute transport occur in both domains. The dual-permeability formulation is based on a set of equations that describe water flow and solute transport separately in each domain (matrix and macropore domains). Numerical models based on the multi-modality of the soil porous system are very useful for the assessment of soil and groundwater contamination from point and diffused sources.

An alternative approach to dual-porosity and dual-permeability models can be to use composite bimodal soil hydraulic property models in the single-porosity flow and transport models (e.g., Othmer et al., 1991; Durner, 1994; Mohanty et al., 1997; Coppola et al., 2009-this issue) that can account for a significant increase in the hydraulic conductivity near saturation. However, these models do not by themselves lead to preferential flow, since when used in a single-domain model based on the Richards equation, simulations will still produce uniform wetting fronts, although possibly with some accelerated advance of the front for surface ponding conditions because of the higher saturated conductivity. Such models, however, cannot predict preferential flow since there is no mechanism to account for lateral nonequilibrium in terms of water moving primarily through larger pores or fractures and bypassing the matrix pore-space (Šimůnek et al., 2003).

Water flow and pesticide transport in soils has been recently studied, both experimentally and numerically, by Köhne et al. (2005, 2006a,b), Pot et al. (2005), Gärdenäs et al. (2006), Kodešová et al. (2005, 2008), and Dousset et al. (2007). These studies showed that pesticide transport is frequently affected by preferential flow due to the presence of macropores. All these studies also considered pesticide application on the top of humic horizons, where pesticide adsorption and degradation are higher than in deeper horizons due to the presence of organic matter and microorganisms. In these studies, it was often observed that pesticides pass through the top humic horizon and contaminate horizons below relatively quickly.

The objective of the current study was to evaluate flow and transport in both the top and underlying soil horizons. For this purpose, undisturbed soil samples were taken from various diagnostic horizons of three different soil types and subjected to various analyses. Configurations of the soil porous system, soil aggregate stability, water and pesticide transport were investigated on all samples to assess either protective or non-protective functions of various soil horizons with respect to groundwater contamination.

2. Materials and methods

2.1. Soil porous system

The study was performed on Haplic Luvisol (parent material loess), Greyic Phaeozem (parent material loess) and Haplic Cambisol (parent material orthogneiss). The elevations of soil locations above sea level are 272 m for Haplic Luvisol, 276 m for Greyic Phaeozem and 523 m for Haplic Cambisol. Average annual temperatures and average annual precipitations (over 30 years) are 8.5 °C and 618 mm for Haplic Luvisol, 8.6 °C and 578 mm for Greyic Phaeozem, and 7.4 °C and 660 mm for Haplic Cambisol, respectively. A five year rotation system with conventional tillage was used at all locations. Winter barley was planted at all areas when field work was performed on August 9 and 10, 2006. Four soil horizons (Ap 0–35 cm, Bt_1 35–62 cm, Bt_2 62–102 cm, Ck 102–133 cm) were identified in Haplic Luvisol, three horizons (Ap 0–21 cm, Bth 21–27 cm, BCk 27–37 cm, Ck 37–80 cm) in Greyic Phaeozem, and three horizons (Ap 0–32 cm, Bw 32–62 cm, Ck 62–97 cm) in Haplic Cambisol. Large undisturbed soil samples of 10×8×4 cm were taken from each horizon of each soil profile except for the Bth horizon of Greyic Phaeozem (the thickness of this horizon was only 5 cm). Micromorphological properties characterizing the soil pore structure were studied on thin soil sections prepared from the soil samples. The final thin section size was approximately 7×4 cm. Two thin sections were made from each soil sample. The soil porous system was analyzed using the procedure described by Pagliai et al. (1983, 2003, 2004). Two images of each thin section were taken at one magnification at a resolution of 300 dpi. The size of the images was 2048×1536 pixels, and the pixel size was 15.7 μm. The applied method allowed

Author's personal copy

studying pores larger than approximately 40 μm. The shape factor, *SF* [−], was calculated according to Pagliai et al. (1983) using the following equation:

$$SF = \frac{P^2}{4\pi A} \quad (1)$$

where P [L] is the pore perimeter and A [L^2] is the pore area. Pores were divided into different shape groups: regular with *SF* of 1–2, irregular with *SF* of 2–5, and elongated with *SF* larger than 5. These groupings correspond approximately to those used by Bouma et al. (1977). Pores of each shape group were further subdivided into size classes either according to their equivalent pore diameter (regular and irregular pores) or their width (elongated pores) (Pagliai et al., 1983).

2.2. Soil structure stability

The stability of the soil structure was evaluated using the index of water-stable aggregates (Nimmo and Perkins, 2002). Four grams of air dry soil aggregates (segregates) of the size of 2–5 mm was sieved for 3 min in distilled water (sieve 0.25 mm). Aggregates remaining on the sieve were next sieved in sodium hexametaphoshate until only sand particles remained on the sieve. The index of water-stable aggregates, *WSA* [−], was then determined as:

$$WSA = \frac{Wds}{Wds + Wdw} \quad (2)$$

where *Wds* [M] is the weight of aggregates dispersed in dispersing solution and *Wdw* [M] is the weight of aggregates dispersed in distilled water. In addition, organic carbon contents, clay contents and cation exchange capacity, which all affect soil structure stability, were measured.

2.3. Water flow and solute transport experiments

Plastic cylinders with a diameter of 10.5 cm and a height of 13 cm were used to collect undisturbed soil samples. Undisturbed soil samples were taken from the Ap (0–13 cm), Bt_1 (42–55 cm), and Bt_2 (65–78 cm) horizons of Haplic Luvisol, the Ap (0–13 cm) and Ck (46–59 cm) horizons of Greyic Phaeozem, and the Ap (0–13 cm) and Bw (40–53 cm) horizons of Haplic Cambisol. Soil samples were transported into the laboratory where micro-tensiometers Tensior 5 (UMS GmbH, Munich, 2005) for pressure head measurements were installed 4 and 8 cm below the soil surface. Cementation was used to prevent water flow and solute transport between the soil core and plastic cylinder. 10 cm^3 of chlorotoluron solution (198 μg cm^{-3} of chlorotoluron) was applied with an infiltration rate of 0.116 cm min^{-1} on the top of the soil samples. Two ponded infiltration experiments with distilled water were then performed during the following 2 days. The ponding depth was maintained at 1.5 cm. The duration of the infiltration experiment varied between 30 min and 7 h depending on the infiltration rate. The duration of individual experiments was set to study possible chlorotoluron leakage from soil horizons under extreme infiltration conditions, and to evaluate chlorotoluron retention in the soil. Water outflow and solute concentration from the bottom of the soil sample were monitored in time. Solute concentrations were determined using High Performance Liquid Chromatography (HPLC). One day after the second infiltration, all soil samples were cut into 8 layers. The sub-samples were dried and the mass of soil in each layer was measured. The soil was then ground and sieved through the 2-mm sieve. The total amount of chlorotoluron remaining in each soil layer was ascertained as follows. 5 g of the dry soil was placed into the centrifuge curette. 5 ml of methanol was added and the centrifuge cuvette was placed for 15 h into the shaking apparatus. After that, analyzed soil samples were centrifuged for 30 min at 13,800 rpm. The chlorotoluron concentration in the methanol extract was again measured using HPLC. The chlorotoluron concentration in the soil sample was expressed as the total amount of solute per a unit of mass of dry soil (μg g^{-1}). Finally, chlorotoluron recovery was found by comparing the amount of applied solute with the sum of solute leached at the bottom of the column and remaining in the soil.

2.4. Numerical evaluation of experimental data

2.4.1. Single-porosity and dual-permeability water flow models

Water flow in the soil profile may be simulated using the single-porosity and dual-permeability models implemented in HYDRUS-1D (Šimůnek et al., 2008a,b). The Richards equation, describing the one-dimensional isothermal Darcian flow in a variably saturated rigid porous medium, is used in both models.

The Richards equation is used to describe water flow in the single-porosity system:

$$\frac{\partial \theta}{\partial t} = \frac{\partial}{\partial z}\left(K(h)\frac{\partial h}{\partial z} + K(h)\right) \quad (3)$$

where θ is the volumetric soil water content [L^3L^{-3}], h is the pressure head [L], K is the hydraulic conductivity [LT^{-1}], t is time [T], and z is the vertical axes [L]. Eq. (3) is solved for the entire flow domain using one set of soil water retention and hydraulic conductivity functions.

In the case of the dual-permeability model, the Richards equation is applied separately to each of the two pore regions, i.e., the macropore (fractures, a domain of larger pores) and matrix domains (Gerke and van Genuchten, 1993):

$$\begin{aligned}\frac{\partial \theta_f}{\partial t} &= \frac{\partial}{\partial z}\left(K_f(h_f)\frac{\partial h_f}{\partial z} + K_f(h_f)\right) - \frac{\Gamma_w}{f_w}\\ \frac{\partial \theta_m}{\partial t} &= \frac{\partial}{\partial z}\left(K_m(h_m)\frac{\partial h_m}{\partial z} + K_m(h_m)\right) + \frac{\Gamma_w}{1-f_w}\end{aligned} \quad (4)$$

where subscripts f and m refer to the macropore and matrix domains, respectively. Γ_w is the mass transfer term for water exchange between the macropore and matrix domains [T^{-1}] and f_w is the macropore domain fraction [−], that is, the ratio of the volume of the macropore domain and the total flow domain. The matrix domain fraction is specified as one minus f_w. Eq. (4) is solved using two sets of soil water retention and hydraulic conductivity functions, which are defined for each domain. The total soil water content or hydraulic conductivity are defined as a sum of the soil water contents or hydraulic conductivities of each domain multiplied by corresponding domain fractions. The mass exchange between the matrix and macropore regions, Γ_w, is calculated using the following equation:

$$\Gamma_w = \frac{b}{a^2} K_a \gamma_w (h_f - h_m) \quad (5)$$

Author's personal copy

where K_a is the effective saturated hydraulic conductivity of the interface between the two pore domains [LT^{-1}]. Parameters describing aggregate shapes are the shape factor b [−] (=15 for spherical aggregates, =3 for cubic aggregates), the characteristic length of an aggregate a [L] (a sphere radius or half size of the cube edge), and the dimensionless scaling factor γ_w [−] (=0.4).

Analytical expressions proposed by van Genuchten (1980) for the soil water retention curve, $\theta(h)$, and the hydraulic conductivity function, $K(\theta)$, are used in both models:

$$\theta_e = \frac{\theta(h)-\theta_r}{\theta_s-\theta_r} = \frac{1}{\left(1+|\alpha h|^n\right)^m}, h<0 \tag{6}$$

$$\theta_e = 1, h\geq 0$$

$$K(\theta) = K_s\theta_e^l\left[1-\left(1-\theta_e^{1/m}\right)^m\right]^2, h<0 \tag{7}$$

$$K(\theta) = K_s, h\geq 0$$

where θ_e is the effective soil water content [−], K_s is the saturated hydraulic conductivity [LT^{-1}], θ_r and θ_s are the residual and saturated soil water contents [L^3L^{-3}], respectively, l is the pore-connectivity parameter [−], α is reciprocal of the air-entry pressure head, [L^{-1}], and n [−] is related to the slope of the retention curve at the inflection point, and $m=1-1/n$ [−].

2.4.2. Single-porosity and dual-permeability solute transport models

Models for solute transport correspond conceptually to the water flow models described above. The single advection–dispersion equation for solute transport is used for the single-porosity system:

$$\frac{\partial\theta c}{\partial t} + \frac{\partial\rho_d s}{\partial t} = \frac{\partial}{\partial z}\left(\theta D\frac{\partial c}{\partial z}\right) - \frac{\partial qc}{\partial z} - \Phi \tag{8}$$

where c [ML^{-3}] and s [MM^{-1}] are solute concentrations in the liquid and solid phases, respectively, q is the volumetric flux density [LT^{-1}], ρ_d is the soil bulk density [ML^{-3}], D is the dispersion coefficient [L^2T^{-1}], and Φ describes zero- and first-order rate reactions [$ML^{-3}T^{-1}$].

The dual-permeability formulation for solute transport is based on two advection–dispersion equations:

$$\begin{aligned}\frac{\partial\theta_f c_f}{\partial t} + \frac{\partial\rho_{d,f} s_f}{\partial t} &= \frac{\partial}{\partial z}\left(\theta_f D_f\frac{\partial c_f}{\partial z}\right) - \frac{\partial q_f c_f}{\partial z} - \Phi_f - \frac{\Gamma_s}{f_w}\\ \frac{\partial\theta_m c_m}{\partial t} + \frac{\partial\rho_{d,m} s_m}{\partial t} &= \frac{\partial}{\partial z}\left(\theta_m D_m\frac{\partial c_m}{\partial z}\right) - \frac{\partial q_m c_m}{\partial z} - \Phi_m + \frac{\Gamma_s}{1-f_w}\end{aligned} \tag{9}$$

where subscripts f and m refer to the macropore and matrix domains, respectively. The mass transfer term for solute exchange between the macropore and matrix domains, Γ_s [$ML^{-3}T^{-1}$], is described using the following equation:

$$\Gamma_s = \frac{b}{a^2}D_e(1-f_w)\theta_m\left(c_f-c_m\right) + \Gamma_w c^* \tag{10}$$

where D_e is the effective diffusion coefficient [L^2T^{-1}] and c^* is equal either to c_f for $\Gamma_w>0$ or to c_m for $\Gamma_w<0$.

Assuming equilibrium solute adsorption, the equilibrium isotherm relating the sorbed concentration, s, to the aqueous concentration, c, can be described using the Freundlich equation:

$$s = k_F c^\beta \tag{11}$$

where k_F and β are empirical coefficients. This equation is valid for both single-porosity and dual-permeability models.

Nonequilibrium solute adsorption may also be simulated using the two-site sorption concept (van Genuchten and Wagenet, 1989). The adsorbed concentration of solute on soil particles may be defined as:

$$s = s_e + s_k \tag{12}$$

where s_e [MM^{-1}] denotes the adsorbed solute concentration on equilibrium sorption sites in the solid phase and s_k [MM^{-1}] represents the remaining solute concentration adsorbed to the solid phase by a slow time-dependent process. The first-order rate equation for kinetic solute sorption is written as:

$$\frac{\partial s_k}{\partial t} = \omega_c\left[(1-f_s)k_F c^\beta - s_k\right] \tag{13}$$

where ω_c [T^{-1}] is the first-order sorption rate constant, f_s [−] is the fraction of equilibrium sorption sites, and k_F and β are parameters of the Freundlich adsorption isotherm.

2.4.3. Estimation of soil hydraulic properties

The single-porosity model in HYDRUS-1D was first used to analyze transient infiltration data (cumulative infiltration, cumulative outflow and pressure heads at two positions) to obtain the parameters of both soil hydraulic functions (soil water retention and unsaturated hydraulic conductivity functions) that were described using the van Genuchten model (Eqs. (6) and (7)). Only the initial part (up to 150 min) of the first ponding infiltration experiment was analyzed to reduce the impact of changes in the soil structure and consequently in the porous system. Initial conditions within the soil sample were set based on pressure heads measured at the beginning of the experiments. Pressure heads at monitored locations were set to measured values, while pressure heads between, above, and below were linearly interpolated and/or extrapolated. Since the soil samples were stored vertically in plastic bags at a cold place for 4 weeks before experiments, the initial conditions were close to hydrostatic conditions. The upper boundary condition was defined using an initial infiltration pulse of 0.116 cm min^{-1} and a duration of 1 min, followed by a constant pressure head of 1.5 cm. The bottom boundary condition was defined using a seepage face.

While the saturated water content, θ_s, was set equal to the measured porosity, the remaining soil hydraulic parameters (i.e., θ_r, α, n, and K_s) were optimized. In all cases the pore connectivity parameter was assumed to be equal to an average value for many soils (l=0.5) (Mualem, 1976) since it was found (not shown) that optimization of the l parameter increased uncertainty for all optimized parameters.

The dual-permeability model of Gerke and van Genuchten (1993), as implemented in HYDRUS-1D, was applied next. Two scenarios (DPM1 and DPM2) that were considered are described below. To obtain unique optimization results for this complex model, many of its parameters must be set equal to

Author's personal copy

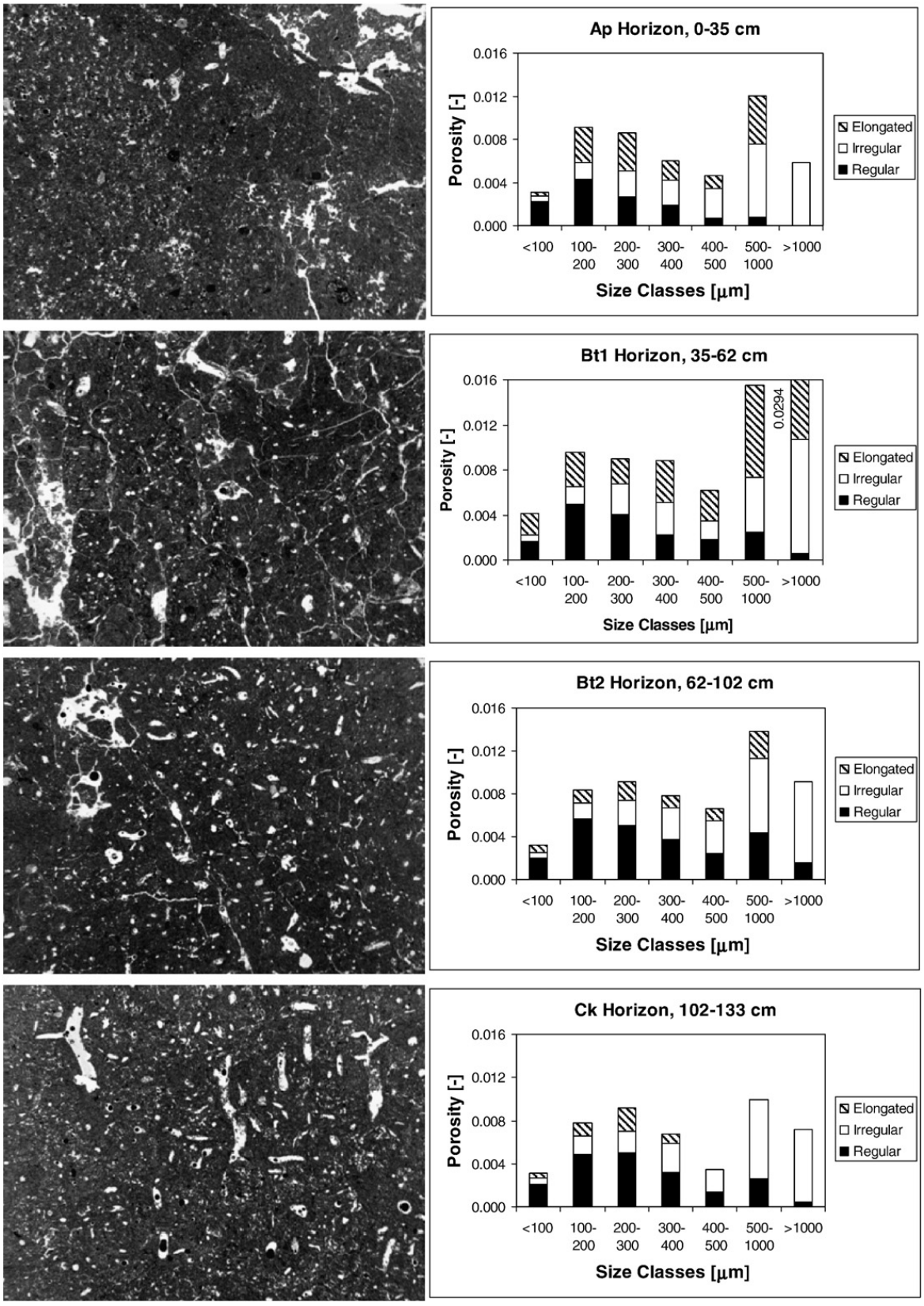

Fig. 1. Images of soil-pore structure (left; frame length of 32.1 mm) and pore size and shape analysis (right) for various horizons of Haplic Luvisol.

independently estimated values. In both cases, the fraction of the macropore domain was estimated using the fraction of pores identified from micromorphological images. The following parameters were used to define the structure of both domains: $b=5$ (the shape factor characterizing angular blocky aggregates), $a=0.2$ cm, and $\gamma_w=0.4$. Saturated water contents of the matrix and macropore domains, $\theta_{s,m}$ and $\theta_{s,f}$, respectively, were assumed to be the same and equal to the measured porosity. The residual

Author's personal copy

water content of the macropore domain, $\theta_{r,f}$, was set to zero. In the DPM1 scenario, it was assumed that large pores control saturated water flow and that the K_s value obtained via numerical inversion using the single porosity model can be used to derive the saturated hydraulic conductivity of the macropore domain, $K_{s,f}$, as a ratio of K_s and the macropore domain fraction, f_w. The remaining parameters $\theta_{r,m}$, α_m, n_m, $K_{s,m}$, α_f, n_f, and K_a were optimized. In the DPM2 scenario, the n_f parameter was set equal to a value of 2.5 to define the step-like shape retention curve that is characteristic for macropores. The remaining parameters $\theta_{r,m}$, α_m, n_m, $K_{s,m}$, α_f, $K_{s,f}$ and K_a were optimized. In all cases, parameters n were restricted to vary between 1.1 and 3.

2.4.4. Estimation of solute transport parameters

Solute transport parameters were estimated using measured outflow concentrations versus time for the single-porosity and dual-permeability models. In the case of the single-porosity model, two scenarios (SPM-S1 and SPM-S2) were simulated. Initial and boundary water flow conditions were defined as before. Soil hydraulic parameters obtained from previous inversions of water flow data were fixed. In addition, a solute concentration of 198 μg cm^{-3} was specified for the initial infiltration pulse (1 min). A zero concentration gradient was defined at the bottom of the sample. Chlorotoluron adsorption in different soil horizons was studied on undisturbed soil samples using the standard laboratory procedure and adsorption isotherms were described using the Freundlich Eq. (11). Bulk density was set to the measured value. Molecular diffusion was assumed to be zero. In the SPM-S1 scenario, only the longitudinal dispersivity was optimized. The two-site sorption concept (van Genuchten and Wagenet, 1989) was applied in the SPM-S2 scenario to characterize nonequilibrium solute adsorption. Due to the fact that experiments often do not provide enough information to optimize all remaining parameters, the

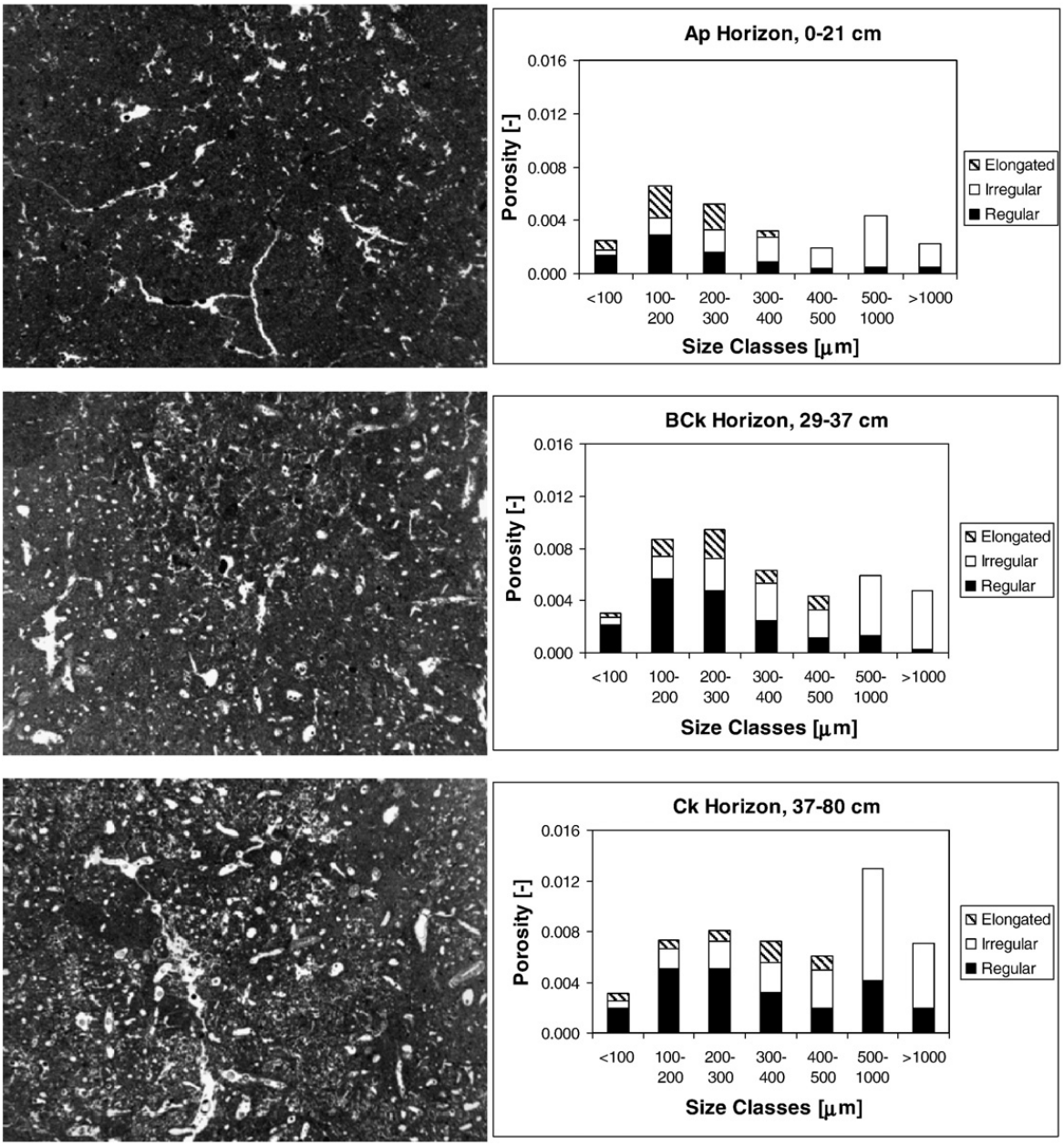

Fig. 2. Images of soil-pore structure (left; frame length of 32.1 mm) and pore size and shape analysis (right) for various horizons of Greyic Phaeozem.

Author's personal copy

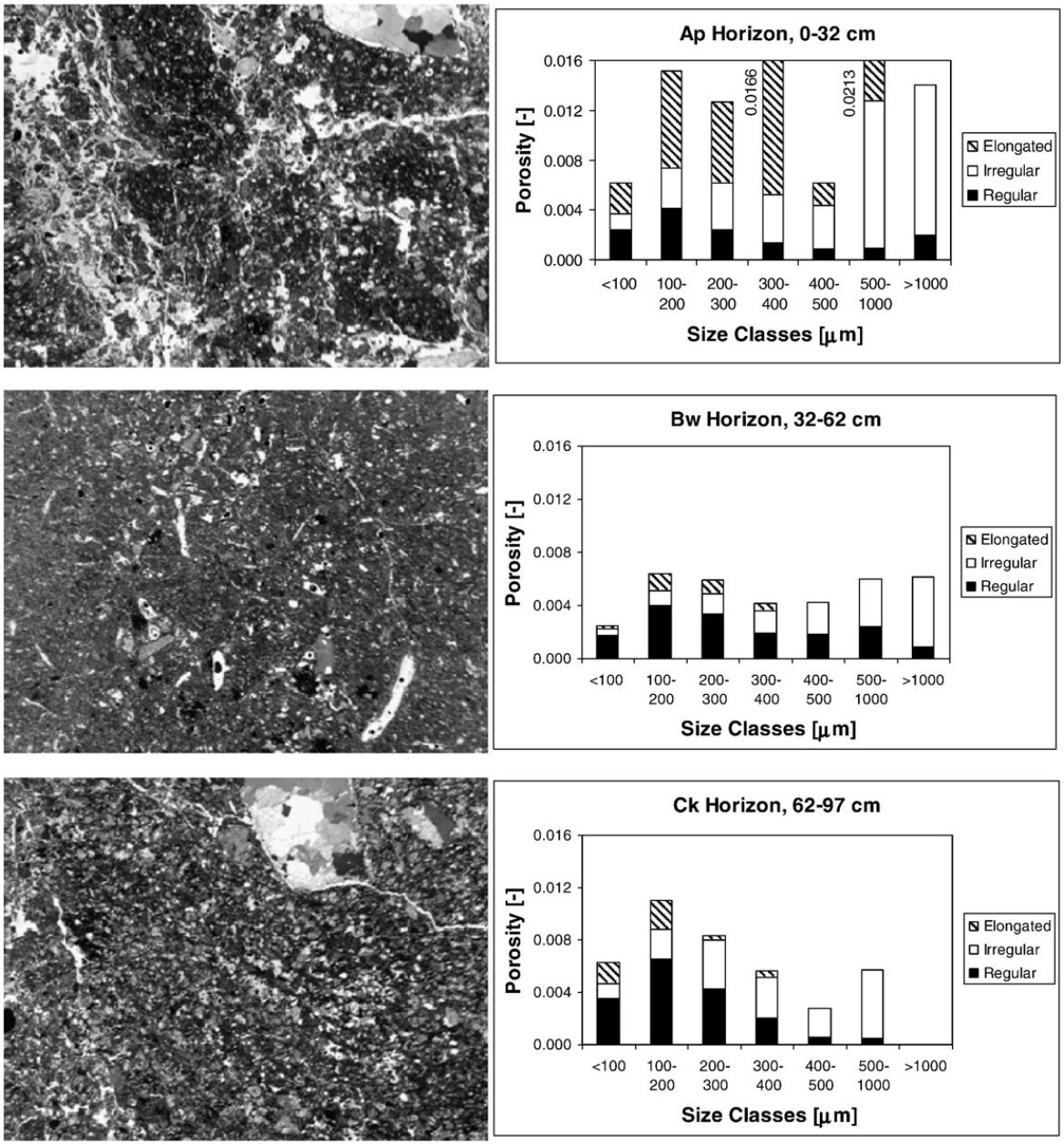

Fig. 3. Images of soil-pore structure (left; frame length of 32.1 mm) and pore size and shape analysis for (right) various horizons of Haplic Cambisol.

ω_c parameter was set to 0.0001 min^{-1}, as found by Köhne et al. (2006a,b). The longitudinal dispersivity and parameter f_s were optimized using measured transient solute transport data in the SPM-S2 scenario.

Two scenarios (DPM-S1 and DPM-S2) were also considered using the dual-permeability model. Initial and boundary condition were specified in the same way as for the single-porosity model. The fraction of surface flow into the macropore

Table 1
Total image porosities and portion of different pore sizes

Soil type	Horizon	Image porosity	Portion [%] of different size classes [µm]						
			<100	100–200	200–300	300–400	400–500	500–1000	>1000
Haplic Luvisol	Ap	0.0494	6.3	18.5	17.4	12.2	9.4	24.4	11.8
	Bt_1	0.0826	4.9	11.6	10.9	10.7	7.5	18.8	35.6
	Bt_2	0.0582	5.4	14.4	15.8	13.5	11.4	23.7	15.8
	Ck	0.0475	6.7	16.3	19.4	14.2	7.3	20.9	15.2
Greyic Phaeozem	Ap	0.0386	7.1	22.4	12.6	16.6	6.7	22.0	12.6
	BCk	0.0424	7.2	20.4	22.4	14.8	10.2	13.9	11.1
	Ck	0.0519	6.0	14.1	15.6	13.9	11.7	25.0	13.5
Haplic Cambisol	Ap	0.0920	6.7	16.4	13.8	18.1	6.6	23.1	15.3
	Bw	0.0354	7.1	18.1	16.8	11.7	11.9	17.1	17.3
	C	0.0396	15.8	27.6	21.0	14.1	7.0	14.5	0.0

Author's personal copy

Table 2
Index of water stable aggregates (WSA) and soil properties affecting aggregate stability

Soil type	Horizon	WSA index [−]	Organic carbon content [%]	Clay content [%]	Cation exchange capacity [mmol$^+$(100 g)$^{-1}$]
Haplic Luvisol	Ap	0.48	1.11	24.4	14.0
	Bt_1	0.61	0.50	34.7	21.2
	Bt_2	0.30	0.32	33.7	25.5
	Ck	0.05	0.17	24.0	16.5
Greyic Phaeozem	Ap	0.56	1.11	32.6	20.5
	Bth	0.60	0.50	37.3	29.2
	BCk	0.45	0.46	31.0	22.5
	Ck	0.10	0.29	27.6	15.5
Haplic Cambisol	Ap	0.75	1.77	15.0	14.2
	Bw	0.46	0.41	24.6	13.5
	C	0.39	0.37	23.5	15.0

domain was defined as a ratio of $K_{s,f}$ multiplied by the domain fraction and the total saturated hydraulic conductivity (the sum of saturated hydraulic conductivities of both domains multiplied by corresponding domain fractions). Soil hydraulic parameters obtained from the previous inversions (the DPM2 scenario) were again fixed. In both scenarios, the two-site sorption concept was applied to describe the adsorption processes in the matrix domain. Parameters $k_{F,m}$ and β_m were set to measured values. Parameter ω_c was again set equal to 0.0001 min^{-1}. The longitudinal dispersivity and the $f_{s,m}$ parameter were optimized using the measured transient solute transport data and the numerical inversion. In the DPM-S1 scenario, similar to MACRO (Larsbo and Jarvis, 2003), the piston type of solute transport was considered in the macropore domain and the longitudinal dispersivity was set to a low value of 0.01 cm. Chlorotoluron adsorption in the macropore domain was neglected because of a much smaller surface area in contact with solute than in the matrix domain and because of the short contact time in this fast flowing region. In the DPM-S2 scenario, the longitudinal dispersivity in the macropore domain was also optimized. Molecular diffusion was neglected in both domains and both scenarios. Chlorotoluron degradation, which may be defined using the first-order rate reaction, was neglected in all cases due to the short experimental duration.

3. Results and discussion

3.1. Soil porous systems

Depending on the type of pedogenesis, soils exhibit different porous systems. Micromorphological images (one for each soil sample) and pore-size histograms (average for four images) of all horizons of Haplic Luvisol, Greyic Phaeozem, and Haplic Cambisol are shown in Figs. 1–3, respectively. Total image porosities and fractions of different pore sizes are given in Table 1. In all cases, the results demonstrate the multimodality of soil porous systems. Bimodality of soil porous systems detected on these images is more or less evident for all soils and all soil horizons. A limit value between two size class modes is 500 μm. Another domain of considerably smaller pores is expected either in higher order aggregates (in the top humic Ap, and deeper Bt_1 and Bt_2 horizons), or in the homogeneous matrix structure (the Ck, C, BCk and Bw horizons). Pores of different sizes may be classified according to their impact on water flow. A definition of macropores as pores causing the physical non-equilibrium of water flow close to saturation (frequently under ponding conditions) is given in the review paper of Jarvis (2007). He suggested that macropores are pores with an equivalent diameter larger than about 300–500 μm, corresponding to pressure heads of −10 and −6 cm. On the other hand, Kodešová et al. (2006, 2008) showed that even smaller pores may play a significant role. They defined gravitational pores as pores with an equivalent diameter larger than 1470 μm, corresponding to a pressure head of −2 cm (Watson and Luxmoore, 1986), and large capillary pores as pores with a diameter larger than 40 μm (pores detectable on micromorphological images), corresponding to a pressure head of −70 cm, and smaller than 1470 μm. This definition was also based on the bimodal shape of the soil water retention curve (Kodešová at al., 2007) obtained from multiple outflow experiments. The macropore domain in the dual-permeability model of HYDRUS-1D was defined as a domain of large capillary pores. Interestingly, the limiting value between two size class modes documented in Figs. 1–3 is similar to the limiting value for macropores as summarized by Jarvis (2007).

Table 3
Infiltration durations, total volumes of infiltrating water and total volumes of water captured below the soil samples

Soil type	Horizon	Infiltration duration 1st day	Total infiltration 1st day (cm^3)	Total outflow 1st day (cm^3)	Infiltration duration 2nd day	Total infiltration 2nd day (cm^3)	Total outflow 2nd day (cm^3)
Haplic Luvisol	Ap	6 h 54 min	725 [a] (875) [b]	507 [a] (600) [b]	4 h 27 min	25 [a] (60) [b]	10 [a] (29) [b]
	Bt_1	0 h 30 min	2400 (2550)	2092 (2228)	0 h 32 min	950 (1500)	904 (1035)
	Bt_2	4 h 42 min	1275 (1450)	1098 (1199)	0 h 42 min	425 (550)	430 (550)
Greyic Phaeozem	Ap	5 h 5 min	350 (550)	283 (405)	5 h 52 min	100 (200)	57 (156)
	Ck	3 h 2 min	1225 (1400)	1129 (1264)	2 h 51 min	675 (850)	409 (540)
Haplic Cambisol	Ap	6 h 4 min	1705 (1855)	1307 (1470)	5 h 37 min	200 (325)	178 (301)
	Bw	4 h 51 min	300 (425)	92 (207)	2 h 14 min	50 (175)	29 (136)

[a] Observed during the monitored infiltration period.
[b] Total (during and after infiltration).

Author's personal copy

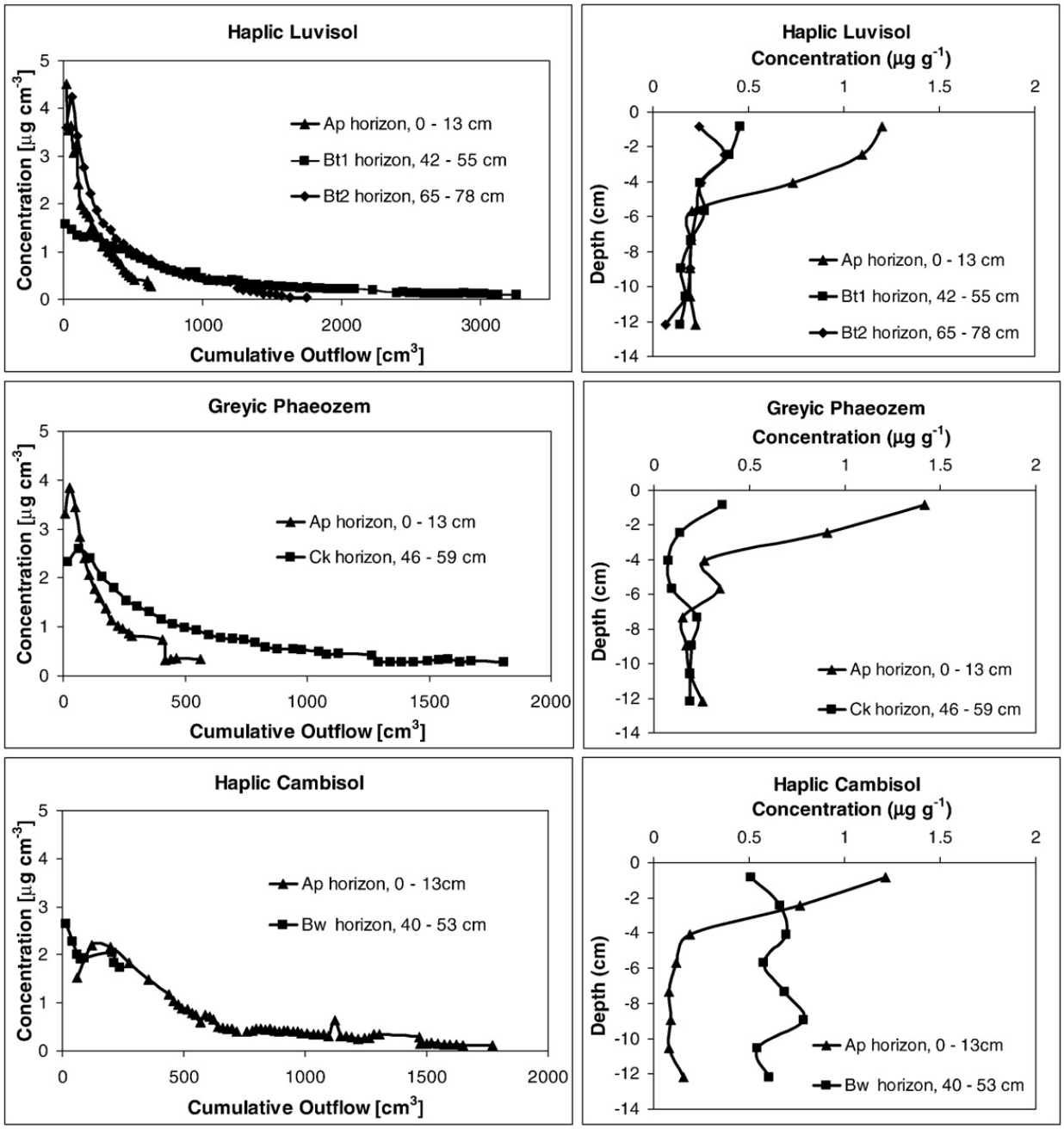

Fig. 4. Cumulative outflow from the bottom of soil samples versus chlorotoluron concentrations (left) and final chlorotoluron concentration distributions (right) for Haplic Luvisol (top), Greyic Phaeozem (middle), and Haplic Cambisol (bottom).

However, an approach proposed by Kodešová et al. (2006) is applied in this study.

The highest porosity in Haplic Luvisol (Fig. 1) was detected in the Bt_1 horizon due to a well-developed prismatic structure that caused a significant increase in fractions of pores with sizes larger than 500 μm. In addition, many elongated pores were observed in this horizon. Their presence in the soil sample may increase water flux through the soil under saturated conditions.

Table 4
Chlorotoluron mass balances in solutes captured below the soil samples and remaining in soils

Soil type	Horizon	Chlorotoluron content in outflow (μg)	Chlorotoluron content in soil (μg)	Recovered chlorotoluron content (μg)	Recovered chlorotoluron (%)
Haplic Luvisol	Ap	857	818	1675	84.6
	Bt_1	1387	360	1747	88.3
	Bt_2	1484	283	1767	89.2
Greyic Phaeozem	Ap	671	788	1459	73.7
	Ck	1443	265	1708	86.3
Haplic Cambisol	Ap	1251	522	1773	89.5
	Bw	672	1025	1697	85.7

Author's personal copy

Table 5
Soil sample porosities, image porosities, and fraction of large pore and macropore domains

Soil type	Horizon	Bulk density [g cm^{-3}]	Specific density [g cm^{-3}]	Porosity of soil sample [−]	Image porosity [−]	Fraction of large pore and macropore domains, f_w [−] [a]
Haplic Luvisol	Ap	1.39	2.43	0.4280	0.0494	0.115
	Bt_1	1.31	2.53	0.4805	0.0826	0.172
	Bt_2	1.23	2.53	0.5119	0.0582	0.114
Greyic Phaeozem	Ap	1.48	2.51	0.4117	0.0386	0.094
	Ck	1.29	2.53	0.4947	0.0519	0.105
Haplic Cambisol	Ap	1.46	2.39	0.3882	0.0920	0.237
	Bw	1.41	2.39	0.4127	0.0354	0.086

[a] A ratio of the overall soil sample porosity and image porosity.

All pores are affected by clay coatings and infillings (Kodešová et al., 2006) that control the water flow interaction between the larger pores and pores of the matrix structure. The largest porosity in Greyic Phaeozem (Fig. 2) was detected in the Ck horizon, again due to an increase in fractions of pores with sizes larger than 500 µm. While a majority of the soil pores were regular or irregular, only a limited number of elongated pores were observed. Lower water fluxes under saturated condition are expected in these soils. Images in Fig. 2 show the relatively homogeneous matrix structure and a system of larger pores created by roots and soil organisms. The highest porosity in Haplic Cambisol (Fig. 3) was detected in the Ap horizon. Despite the fact that aggregates in this horizon are poorly developed, the porous system does not show intrapedal or interpedal pores, and pores are developed mainly along gravel particles, images show many elongated pores of all detectable pore sizes. Comparing all soil horizons (Table 1), the largest image porosity was detected in the Ap horizon of Haplic Cambisol. A slightly lower porosity was observed in the Bt_1 horizon of Haplic Luvisol, but a greater fraction of pores larger than 500 µm was also detected. The lowest porosity was observed in the Bw and C horizons of Haplic Cambisol and no pores of a size larger than 1000 µm were detected in the C horizon.

3.2. Soil structure stability

The indexes of water-stable aggregates, organic carbon contents, clay contents and cation exchange capacities of all horizons in all soil profiles are shown in Table 2. The most stable aggregates in Haplic Luvisol were found in the Bt_1 horizon, presumably because of the presence of clay coatings in this horizon. The stability of the soil structure of the Ap horizon (where the high organic carbon content should insure a high soil aggregate stability) was probably reduced by the agricultural practices. The impact of tillage and clay coatings on soil structure stability within the soil profile is also evident in Greyic Phaeozem. The highest aggregate stability was found in the Bth horizon. In the case of Haplic Cambisol, the soil aggregate stability in the Ap horizon was higher than in deeper horizons (Bw, C), due to higher organic carbon content. A relatively high aggregate stability was found despite micromorphological images showing weakly developed soil aggregates. This was probably also caused by the presence of free iron oxides in this soil.

3.3. Water flow and solute transport experiments

The infiltration durations, total volumes of infiltrating water, and total volumes of water captured below the soil samples are shown in Table 3. Observed infiltration and outflow rates partly reflected the soil structure of various horizons (Figs. 1–3). The highest infiltration rate was observed for the Bt_1 horizon of Haplic Luvisol exhibiting a well-developed prismatic structure. A dense network of large capillary pores with clay coatings and gravitational pores caused significant preferential flow. The irregular, nonuniform flow path geometry for infiltration in structured soils has also been discussed by German and Hensel (2006). The lowest infiltration rate was measured for the Bw horizon of Haplic Cambisol, which displayed a poorly developed soil structure and had no gravitational pores. Lower infiltration rates were observed for the humic Ap horizons of Haplic Luvisol and Greyic Phaeozem than for their subhorizons. On the other hand, a higher infiltration rate was monitored for the humic Ap horizon than for the subhorizon of Haplic Cambisol. Infiltration rates for humic horizons of all three soil types increased due to the presence of macropores as follows: Greyic Phaeozem, Haplic Luvisol, and Haplic Cambisol. In all cases, except for the Bt_2 horizon, infiltration rates during the

Table 6
Soil hydraulic parameters (van Genuchten, 1980) for the single-porosity model

Soil type	Horizon	θ_r [cm^3 cm^{-3}]	θ_s [cm^3 cm^{-3}]	α [cm^{-1}]	n [−]	K_s [cm min^{-1}]	R^2
Haplic Luvisol	Ap	0 [a]	0.4280 [b]	0.0124±0.0010 [c]	2.001±0.173	0.0377±0.0031	0.9454
	Bt_1	0.0102±0.0413	0.4805 [b]	0.0185±0.0206	1.101±1.260	0.8141±0.0951	0.5036
	Bt_2	0.0018±0.0146	0.5119 [b]	0.0114±0.0039	1.221±0.095	0.0694±0078	0.4699
Greyic Phaeozem	Ap	0.0056±0.0011	0.4117 [b]	0.0599±0.0191	1.126±0.009	0.0178±0.0011	0.8302
	Ck	0.0680±0.0079	0.4947 [b]	0.0169±0.00154	1.093±0.009	0.0872±0.0023	0.9229
Haplic Cambisol	Ap	0 [a]	0.3882 [b]	0.1035±0.1550	2.276±1.401	0.0968±0.0082	0.6615
	Bw	0.2415±0.0264	0.4127 [b]	0.0072±0.0003	3.000±0.676	0.0069±0.0006	0.9007

[a] Fixed at 0 during optimization.
[b] Not optimized.
[c] 95% confidence interval.

Author's personal copy

second infiltration decreased significantly. The breakdown of soil structure, swelling of clay particles, and/or air entrapment in the soil may cause this decrease in infiltration rates. The restriction of water flow due to the presence of entrapped air has already been described by Císlerová et al. (1988), as well as others. The largest decrease in infiltration rate was observed for the Ap horizon of Haplic Luvisol, in which breakdown of aggregates led to the formation of the less permeable layer at the surface of the soil sample. This occurred despite the fact that the WSA of the Ap horizon (Table 2) was higher than for the Bt_2 and Ck horizons of the same soil profile. A homogeneous matrix structure with a

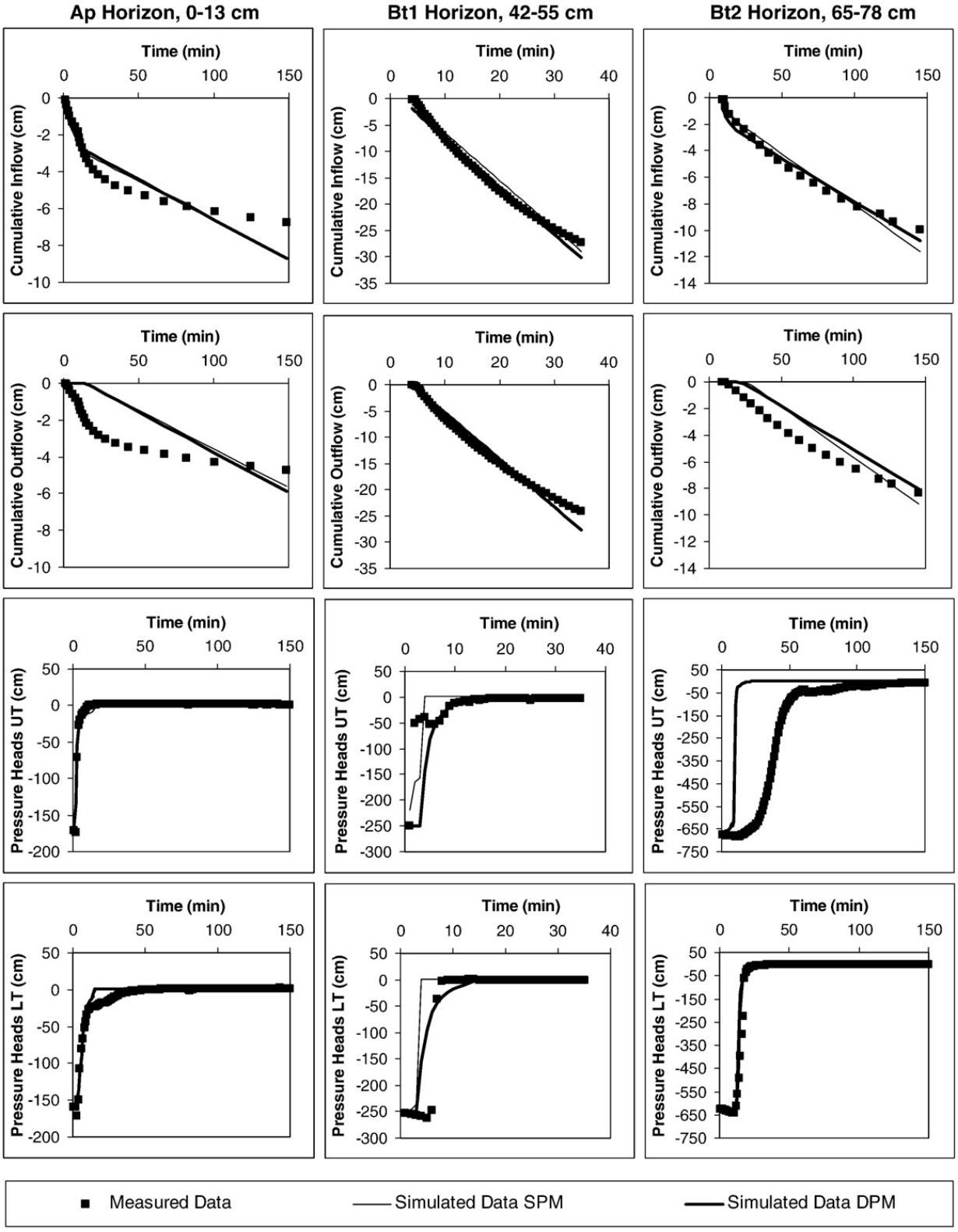

Fig. 5. Cumulative infiltration (Inflow), cumulative outflow (outflow), pressure heads at upper (UT) and lower (LT) tensiometers measured and simulated using the single-porosity (SPM) and dual-permeability (DPM) models (scenario DPM2) for Ap (left), Bt_1 (middle) and Bt_2 (right) horizons of Haplic Luvisol.

Author's personal copy

system of larger pores created by roots and soil organisms in deeper horizons was apparently more stable than the soil aggregates of the Ap horizon.

The relationship between the monitored outflow and outflow chlorotoluron concentrations for all soil samples is shown in Fig. 4. Peak solute concentrations were observed in all cases immediately at or close after the initiation of outflow. Faster infiltration rates usually resulted in lower peak concentrations and a more gradual decrease of measured values. A dense network of large capillary and gravitational pores is likely to have partly bypassed initial chlorotoluron deposits, which were then gradually released into the macropores by mass

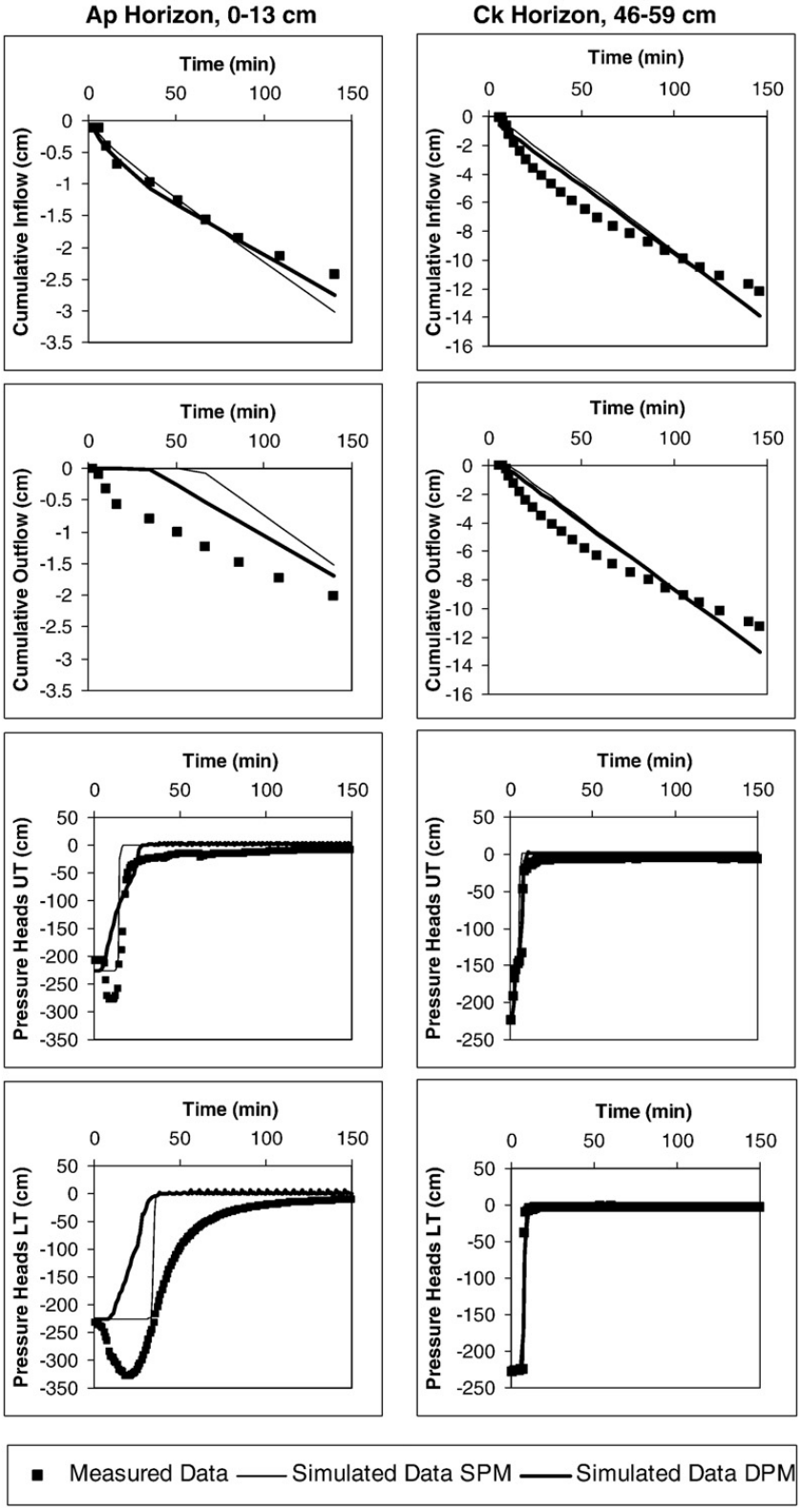

Fig. 6. Cumulative infiltration (Inflow), cumulative outflow (outflow), pressure heads at upper (UT) and lower (LT) tensiometers measured and simulated using the single-porosity (SPM) and dual-permeability (DPM) models (scenario DPM2) for Ap (left) and Ck (right) horizons of Greyic Phaeozem.

Author's personal copy

transfer. Outflow concentrations observed during the second-day infiltration experiments decreased significantly compared to those measured at the end of the first-day infiltration tests. This was likely due to kinetic adsorption processes and mass transfer of chlorotoluron to less mobile zones. Interestingly, chlorotoluron was detected even in the outflow from the Bw horizon of Haplic Cambisol, where a very low outflow was measured.

Final distributions of chlorotoluron concentrations in all soil samples are shown in Fig. 4. The highest chlorotoluron concentrations were found in the surface layers of the Ap horizons of all three soils. A similar phenomenon was also

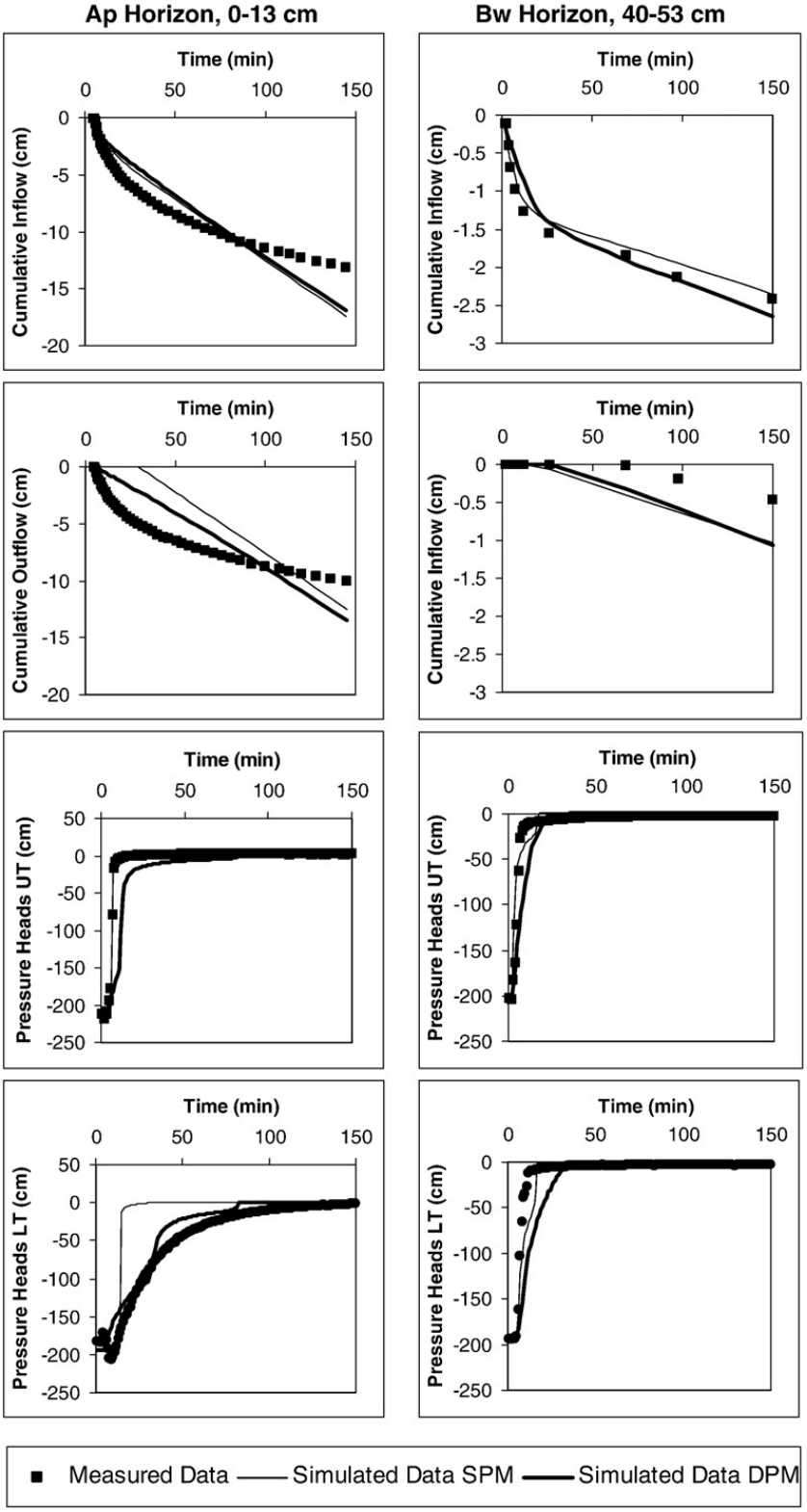

Fig. 7. Cumulative infiltration (Inflow), cumulative outflow (outflow), pressure heads at upper (UT) and lower (LT) tensiometers measured and simulated using the single-porosity (SPM) and dual-permeability (DPM) models (scenario DPM2) for Ap (left) and Bw (right) horizons of Haplic Cambisol.

Author's personal copy

Table 7
Soil hydraulic parameters (van Genuchten, 1980) for the dual-permeability model (scenario DPM1)

Soil type	Horizon	$\theta_{r,m}$ [cm^3 cm^{-3}]	$\theta_{s,m}=\theta_{s,f}$ [cm^3 cm^{-3}]	α_m [cm^{-1}]	n_m [−]	$K_{s,m}$ [cm min^{-1}]	α_m [cm^{-1}]	n_f [−]	$K_{s,f}$ [cm min^{-1}]	K_a [cm min^{-1}]	R^2
Haplic Luvisol	Ap	0.1209±0.1310 [a]	0.4280 [b]	0.0086±0.0010	2.500±1.670	0.0063±0.0026	0.0100±0.0026	3.000±5.080	0.3285 [b]	8.68E−06±5.36E−06	0.9155
	Bt_1	0.1359±0.0172	0.4805 [b]	0.0202±0.0025	1.319±0.176	0.0015±0.0002	0.052±0.0053	1.190±0.137	9.4704 [b]	9.49E−06±1.02E−06	0.6457
	Bt_2	0.1081±0.4220	0.5119 [b]	0.0102±0.0142	1.293±0.295	0.0522±0.0085	0.0137±0.1700	3.000±2.58	0.6080 [b]	3.89E−06±1.25E−04	0.4627
Greyic Phaeozem	Ap	0.1593±0.0269	0.4117 [b]	0.0296±0.0092	1.100±0.086	0.00252±0.0002	0.0319±0.0078	2.851±0.389	0.1900 [b]	1.08E−05±3.00E−06	0.2014
	Ck	0.2003±0.3610	0.4947 [b]	0.0051±0.0055	1.100±0.013	0.0022±0.0027	0.0462±0.0042	2.191±1.800	0.8305 [b]	6.05E−06±3.38E−06	0.9629
Haplic Cambisol	Ap	0.2163±0.0602	0.3882 [b]	0.0267±0.0073	2.501±0.802	0.0051±0.0029	0.0101±0.0148	3.000±0.890	0.4080 [b]	2.03E−07±1.46E−07	0.8421
	Bw	0.2500±0.0149	0.4127 [b]	0.0096±0.0009	1.851±0.165	0.0004±0.0001	0.0103±0.0009	3.000±0.230	0.0802 [b]	3.58E−05±2.43E−06	0.9212

[a] 95% confidence interval.
[b] Not optimized.

Table 8
Soil hydraulic parameters (van Genuchten, 1980) for the dual-permeability model (scenario DPM2)

Soil type	Horizon	$\theta_{r,m}$ [cm^3 cm^{-3}]	$\theta_{s,m}=\theta_{s,f}$ [cm^3 cm^{-3}]	α_m [cm^{-1}]	n_m [−]	$K_{s,m}$ [cm min^{-1}]	α_m [cm^{-1}]	n_f [−]	$K_{s,f}$ [cm min^{-1}]	K_a [cm min^{-1}]	R^2
Haplic Luvisol	Ap	0.1749±0.0185 [a]	0.4280 [b]	0.0225±0.0027	2.418±0.267	0.0233±0.0029	0.0107±0.0015	2.5 [b]	0.1610±0.0205	5.32E−05±6.45E−06	0.9496
	Bt_1	0.1588±0.0177	0.4805 [b]	0.0047±0.0001	1.102±0.018	0.0150±0.0021	0.051±015	2.5 [b]	4.5775±0.1491	1.15E−07±1.24E−08	0.8940
	Bt_2	0.1001±0.0391	0.5119 [b]	0.0102±0.0005	1.294±0.297	0.0528±0.0399	0.0107±0.0102	2.5 [b]	0.1050±0.2650	1.93E−06±7.73E−05	0.4711
Greyic Phaeozem	Ap	0.1875±0.0083	0.4117 [b]	0.0467±0.0024	1.100±0.033	0.0031±0.0001	0.0589±0.0087	2.5 [b]	0.1370±0.0026	9.15E−06±1.16E−06	0.6632
	Ck	0.1735±0.0688	0.4947 [b]	0.0044±0.0002	1.104±0.047	0.0030±0.0023	0.0226±0.0004	2.5 [b]	0.7770±0.025	3.57E−06±1.03E−06	0.9710
Haplic Cambisol	Ap	0.1039±0.1130	0.3882 [b]	0.0267±0.0047	2.505±0.920	0.0085±0.0043	0.0106±0.0139	2.5 [b]	0.3594±0.0237	3.21E−07±2.65E−07	0.8414
	Bw	0.2500±0.0075	0.4127 [b]	0.0265±0.0014	1.635±0.088	0.0002±0.0000	0.0108±0.0003	2.5 [b]	0.0929±0.0036	1.86E−05±9.22E−07	0.8738

[a] 95% confidence interval.
[b] Not optimized.

Author's personal copy

Table 9
Parameters of Freundlich adsorption isotherms determined in the laboratory

Soil type	Horizon	Freundlich adsorption isotherm coefficient, k_F [$cm^{3\beta}\ \mu g^{1-\beta}\ g^{-1}$]	Freundlich adsorption isotherm coefficient, β [–]
Haplic	Ap	2.89	0.80
Luvisol	Bt_1	0.86	0.84
	Bt_2	0.84	0.83
Greyic	Ap	2.73	0.75
Phaeozem	Ck	0.88	0.81
Haplic	Ap	4.77	0.77
Cambisol	Bw	0.52	0.85

observed in the field by Kočárek et al. (2005). This may be explained by solute diffusion into the soil aggregates immediately after the solute application, and a subsequent slow solute release from aggregates into the preferential flow paths, or even solute isolation in the aggregates. Chlorotoluron concentrations in top layers of subsurface horizons were lower than those in the Ap horizons and chlorotoluron was more evenly distributed with depth. Chlorotoluron concentrations within the Bw horizon of Haplic Cambisol were very high due to very low outflow from the soil sample. Despite this low outflow, chlorotoluron was regularly distributed within the soil profile.

Chlorotoluron amounts captured in the outflow from soil samples and remaining in soils are presented in Table 4. As expected, higher chlorotoluron contents in outflow were found for samples with higher cumulative outflow. The highest chlorotoluron content remaining in the soil was found for the Bw horizon of Haplic Cambisol, due to very low outflow. Chlorotoluron recovery varied for different soil samples. The highest chlorotoluron recovery was found for soil samples with high infiltration rates. Chlorotoluron recovery was partly affected by pesticide degradation, which was assumed to be between 5 and 8% of the applied mass. Pesticide losses during sample segmentation, soil sample grinding and sieving, incomplete pesticide dissolution in methanol, heterogeneity of applied solute, and measurement errors are other likely reasons for incomplete chlorotoluron recovery.

3.4. Numerical evaluation of experimental data

3.4.1. Estimation of soil hydraulic properties

Soil sample porosities evaluated from bulk densities (calculated for the entire 1125.1-cm^3 undisturbed soil sample) and specific densities are presented in Table 5. Soil hydraulic parameters obtained using numerical inversions of the transient flow data and the single-porosity model and R^2 of measured and simulated data are shown in Table 6. Measured transient outflow data (Figs. 5–7) were, in most cases, not satisfactorily described by the model. In all cases, water outflow was observed almost immediately after the beginning of the ponding infiltration. The later wetting front breakthrough was simulated especially in all Ap horizons. While simulated infiltration and outflow rates remained constant after the wetting front breakthrough, observed infiltration and outflow rates decreased with time due to the breakdown of the soil structure and changes in particle volumes. As discussed above, the soil structure breakdown (occurred as the soil surface collapsed) was most evident in the soil sample taken from the Ap horizon of Haplic Luvisol. In several cases (especially those with the lowest R^2), while simulated pressure heads indicated a fast advance of the wetting front, the observed data demonstrated a much slower wetting front movement. Measured pressure heads likely characterized pressure heads in the matrix domain that may represent either immobile domains or domains with very low permeability. Confidence intervals (95%) for the optimized K_s parameter show that this parameter can be estimated from the infiltration experiment highly reliably. On the other hand, 95% confidence intervals for some other optimized parameters were very wide, indicating that observed data were affected by the factors discussed above, and that the single porosity model was not suitable to describe the flow process in studied soils.

The soil hydraulic parameters for all soils obtained using the numerical inversion of the dual-permeability model and R^2 of measured and simulated data are shown in Tables 7 and 8 for scenarios DPM1 and DPM2, respectively. As discussed above, fractions of large capillary pore and gravitational pore domains (Table 5) were defined as a ratio of the image porosity and the soil sample porosity. R^2 values in Table 8 show that correlations between measured and simulated data are better for Haplic Luvisol and Greyic Phaeozem when using the DPM2 scenario and slightly better for Haplic Cambisol when using the DPM1 scenario. However, 95% confidence intervals show that optimized parameters are more reliable for the DPM2 scenario in all cases. Similarly as for the single-porosity model, dynamic parameters (i.e., $K_{s,m}$ and $K_{s,f}$) are determined better than other optimized parameters. Despite the large number of optimized parameters this experiment provides enough information about the saturation water fluxes. Another factor that increases the uncertainty of optimized parameters, apart from those already discussed earlier, is the fact that the experiments were performed under conditions close to soil saturation, and consequently the wetting front moved very fast. Pressure heads ranged from −250 to 0 cm during all infiltration experiments, except for the Bt_2 horizon of Haplic Cambisol

Table 10
Solute transport parameters obtained using the numerical optimization with the single-porosity model

		Scenario SPM-S1		Scenario SPM-S2		
Soil type	Horizon	Longitudinal dispersivity [cm]	R^2	Longitudinal dispersivity [cm]	The fraction of equilibrium sorption sites, f_s [–]	R^2
Haplic Luvisol	Ap	40.000±0.004	0.3916	40.000±14.00	0.140±0.172	0.4420
	Bt_1	40.000±0.010	0.8418	38.242±9.942	0.826±0.121	0.8607
	Bt_2	40.000±0.016	0.0059	40.000±0.022	0.340±0.509	0.0333
Greyic Phaeozem	Ap	40.000±540.0	0.1760	36.523±321.10	0.039±0.419	0.1768
	Ck	40.000±0.040	0.0083	17.751±15.500	0.109±0.123	0.1527
Haplic Cambisol	Ap	7.454±0.094	0.2248	40.000±5.850	0.900±0323	0.5897
	Bw	26.408±0.022	0.7728	4.084±4.510	0.117±3.102	0.9026

Author's personal copy

Table 11
Solute transport parameters obtained using the numerical optimization with the dual-permeability model

Soil type	Horizon	Scenario DPM-S1			Scenario DPM-S2			
		Longitudinal dispersivity in matrix [cm]	The fraction of equilibrium sorption sites in matrix, $f_{s,m}$ [−]	R^2	Longitudinal dispersivity in matrix [cm]	The fraction of equilibrium sorption sites in matrix, $f_{s,m}$ [−]	Longitudinal dispersivity in macropores [cm]	R^2
Haplic Luvisol	Ap	30.70±19.30	0.280±0.379	0.4492	30.00±24.70	0.165±0.395	5.294±7.143	0.4665
	Bt_1	5.620±4.740	0.499±0.243	0.5258	4.010±6.412	0.504±0.894	0.018±0.056	0.5903
	Bt_2	1.828±3.311	0.498±0432	0.0982	8.019±2.000	0.097±1.110	1.399±8.808	0.6330
Greyic Phaeozem	Ap	13.373±66.122	0.473±0.593	0.0169	5.670±116.604	0.502±13.135	0.014±19.457	0.0197
	Ck	40.000±2.990	0.212±0.114	0.7732	40.000±35.100	0.215±0.117	0.023±0.007	0.7956
Haplic Cambisol	Ap	0.365±4.520	0.016±0.009	0.1022	0.538±7.390	0.021±0.164	0.005±0.199	0.1105
	Bw	2.592±5.361	0.334±0.548	0.9357	3.589±1.990	0.505±1.583	0.0003±0.038	0.9396

where they ranged from −700 to 0 cm. Such data may hardly provide enough information to optimize the residual water content, and in some cases (having data for only relatively narrow experimental pressure head interval without information about the dry range), even the optimization of α and n parameters (characterizing the shape of soil hydraulic functions) may be difficult.

A comparison of correlations between measured and simulated data using either the single-porosity or dual-permeability models shows that the R^2 values did not, in some cases, increase for the dual-permeability model. The R^2 value for the Ap horizon of Greyic Phaeozem due to the applied restrictions even significantly decreased. However, Figs. 5–7 show that outflows/inflows simulated using the DPM2 scenario describe observed trends better, such as earlier wetting front breakthrough. Better correlations between measured and simulated pressure heads were not always achieved due to the reasons previously discussed. In addition, the bimodality of the large capillary pore and the gravitational pore fraction detected in micromorphological images, which were not considered in numerical simulations, may have had a significant impact on water flow within soil samples. Dividing a detected pore-flow domain into two domains (a domain of pores with an equivalent diameter larger than 500 μm and a domain of pores with an equivalent diameter smaller than 500 μm), each with its own soil hydraulic properties, would most likely increase the simulated infiltration rate in the domain of large pores and cause earlier wetting front breakthrough. However, such a scenario cannot be simulated using the applied simulation program. It must be also pointed out that the size of the thin soil sections presumably allows for studying capillary pores. Thin soil sections would have to be larger in order to study larger gravitational pores. In addition, a thin soil section provides only a two-dimensional image of the soil porous system. The accidental occurrence of larger gravitational pores and their shape makes it difficult to study them using this technique. The impact of gravitational pores on water flow, which were not detected on micromorphological images, is the most evident in the Ap horizon of Greyic Phaeozem. The influence of gravitational pores significantly increases in soils with lower fractions of pores detectable on micromorphological images. On the other hand, the flow conditions similar to ponding infiltration, which cause water flow through gravitational pores, are not frequently observed in nature. Therefore, soil micromorphological images should provide sufficient information for characterizing flow domains, model selection and definition of soil hydraulic properties under the flow conditions prevailing in nature (Kodešová et al., 2006, 2008).

3.4.2. Estimation of solute transport parameters

The parameters of the Freundlich adsorption isotherm used in all simulations were independently determined in the laboratory using batch experiments (Table 9). Additional optimized solute transport parameters and R^2 coefficients obtained using the single-porosity and dual-permeability

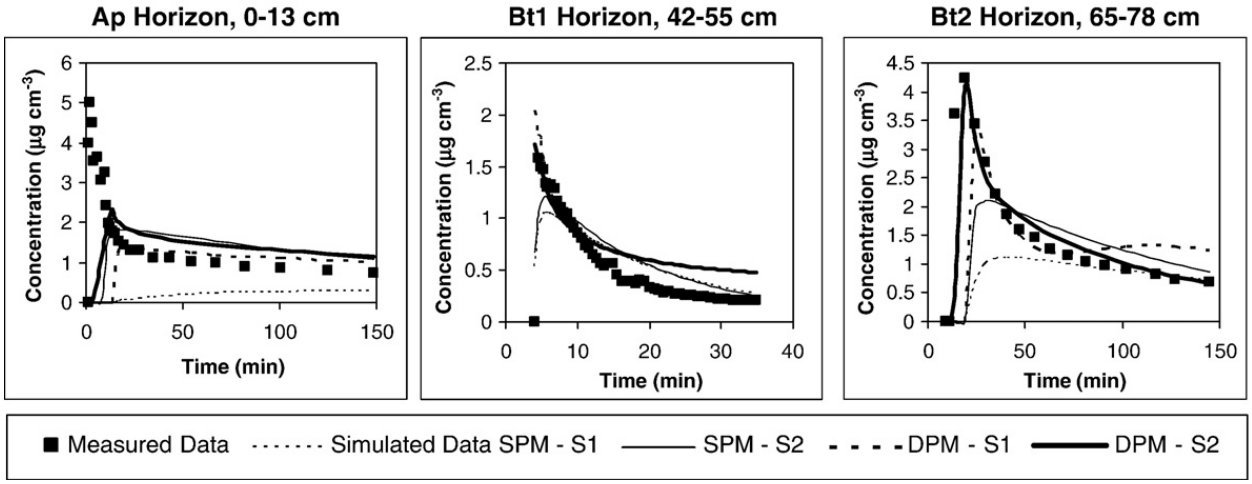

Fig. 8. Outflow concentrations measured and simulated using the single-porosity (SPM) (scenarios SPM-S1 and SPM-S2) and dual-porosity (DP) (scenarios DPM-S1 and DPM-S2) models for Ap (left), Bt_1 (middle) and Bt_2 (right) horizons of Haplic Luvisol.

Author's personal copy

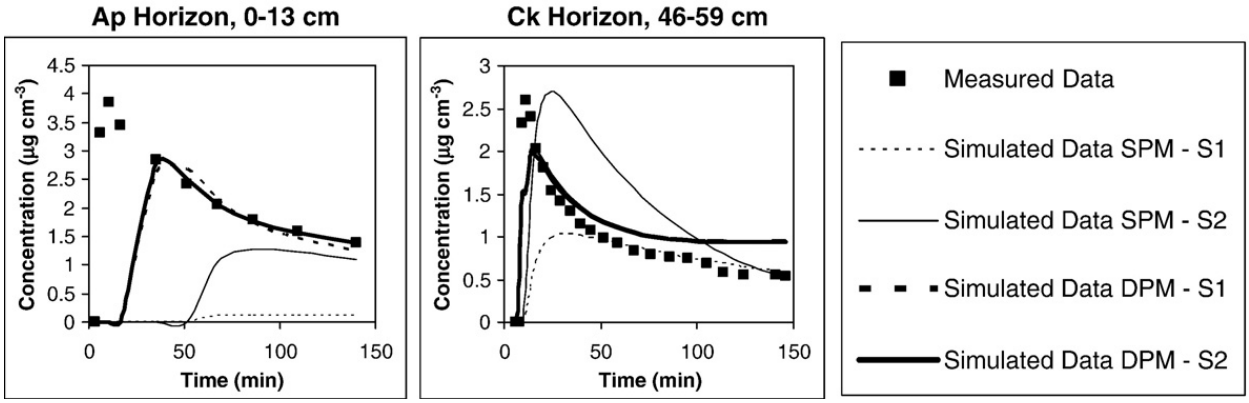

Fig. 9. Outflow concentrations measured and simulated using the single-porosity (SPM) (scenarios SPM-S1 and SPM-S2) and dual-porosity (DPM) (scenarios DPM-S1 and DPM-S2) models for Ap (left) and Ck (right) horizons of Greyic Phaeozem.

models are given in Tables 10 and 11, respectively. Observed and simulated chlorotoluron concentrations for all numerical scenarios and all soil horizons are presented in Figs. 8–10. It is evident that the SPM-S1 scenario (the single porosity model with optimized value of the longitudinal dispersivity) could not simulate observed outflow concentrations for the Ap horizons of all soil types due to the high prescribed sorption (Table 9), and was able to predict only concentration tailing for deeper horizons. Using the concept of two-site sorption improved correspondence between measured and simulated data for deeper horizons. However, it was possible to predict the early chlorotoluron breakthrough only using the dual-permeability model. As with water flow, although the R^2 values did not always indicate improved correlations between measured and simulated data when the dual-permeability model was used, Figs. 8–10 show that the dual-permeability model better described the general trends exhibited by measured concentrations. However, simulated peak concentrations were almost always lower than measured values. Simulated tail concentrations were usually either similar or slightly higher than measured values. A comparison of modelling results obtained by the two dual-permeability scenarios reveals that the DPM-S2 scenario provided better correlations between measured and simulated data, mainly due to the increase in the number of optimized parameters. However, in many cases the value of the optimized longitudinal dispersivity was very low, and similar to the fixed value in the DPM-S1 scenario. Note that several dual-permeability models, such as MACRO (Larsbo and Jarvis, 2003), assume piston-type solute transport in the macropore domain and neglect dispersion in this domain altogether. Again, confidence intervals of many optimized parameters were often very wide, indicating their nonuniqueness and mutual correlations. Changes in soil structure and bimodality of the macropore domain hampered attempts to find a unique set of solute transport parameters that would describe collected transient data. Since it was shown by Köhne et al. (2006b) that adsorption in the macropore domain should be assumed in the horizons containing organic matter, chlorotoluron adsorption in macropores was also simulated (not shown). However, such simulations led to either no correlation between measured and simulated data, or the two-site sorption concept had to be applied again with a very low value of the fraction of equilibrium sorption sites in macropores. In addition, observed data do not provide enough information to optimize so many parameters. Finally, macropores in the subsurface horizons of Haplic Luvisol and the Ap horizon of Greyic Phaeozem were affected by clay coatings that may decrease the pesticide sorption (Celis et al., 1997).

This study showed that even in soils with poorly or undeveloped soil aggregates and without larger gravitational pores (the Bw horizon of Haplic Cambisol) the small fracture of large capillary pores detected in micromorphological images significantly influenced solute transport. The impact of these pores was previously documented by Kodešová et al. (2008), by

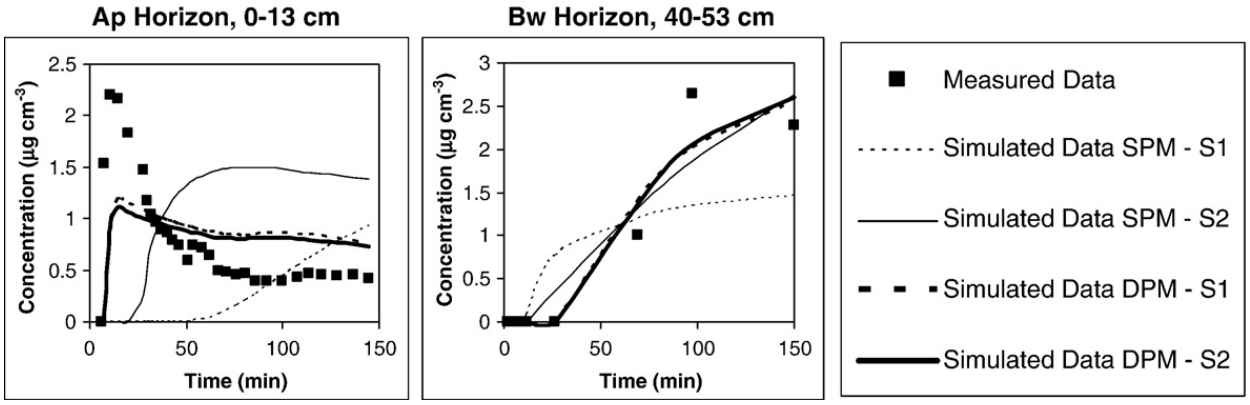

Fig. 10. Outflow concentrations measured and simulated using the single-porosity (SPM) (scenarios SPM-S1 and SPM-S2) and dual-porosity (DPM) (scenarios DPM-S1 and DPM-S2) models for Ap (left) and Bw (right) horizons of Haplic Cambisol.

Author's personal copy

comparing simulated pesticide distribution within the soil profile with pesticide distribution studied experimentally in the field. This assumption was proved here via numerical inversion of laboratory experimental data.

4. Conclusions

Soil pore structure, soil aggregate stability, water flow, and chlorotoluron transport were studied in various diagnostic horizons of three soil types. Observed infiltration and outflow rates and pesticide transport closely reflected the soil structure of the studied horizons. Transport processes were also affected to a certain degree by the breakdown of soil structure. The highest water flow rates were observed in soils with well-developed soil structures, which were affected by clay coatings and high aggregate (structure) stability. The lowest water flow rates were observed in soils with poorly developed soil structures, a low fraction of large capillary pores, and the absence of gravitational pores. Water flux was affected significantly during the experiment by the aggregate breakdown in the well-aggregated soil with moderate aggregate stability. On the other hand, structural changes were less significant in compact homogeneous matrix structures with systems of larger pores created by roots and soil organisms and low structure stability. The dual-permeability model improved the description of collected data in comparison to the single-porosity model. However, better correlations were not always obtained due to the breakdown of soil structure and particle volume changes during experiments. In addition, the bimodality of the large pore and gravitational pore fraction detected in micromorphological images, which was not considered in numerical simulations, may have had a significant impact on water flow in the soil samples. Utilization of the dual-permeability model and the concept of a two-site sorption applied to the matrix domain made it possible to fit the measured data more closely than when the single-porosity model with equilibrium adsorption was used. This study confirmed that chlorotoluron is highly mobile under saturated conditions in the deeper horizons of Haplic Luvisol and Greyic Phaeozem. Interestingly, the parent material for both soils was loess, which is usually assumed to be a low-permeability material. On the other hand, Cambisols are usually assumed to be soils with high permeability due to the presence of preferential pathways. This assumption was not confirmed for deeper horizons of the studied Cambisol. However, the prevailing fast chlorotoluron transport through large capillary pores, and frequently through gravitational pores, was documented in all cases. Micromorphological images and soil porous system analysis significantly improved the understanding of transport processes in studied soils.

Acknowledgement

Authors acknowledge the financial support of the Grant Agency of the Czech Republic (grant No. GA CR 526/08/0434) and the Ministry of Education, Youth and Sports (grants No. 2B06095 and No. MSM 6046070901). The thin section preparation and the image analysis were funded by the Italian Agricultural Ministry (grant No. D.M. 2/7331/06). We also thank to Anna Žigová and Karel Němeček for their help with the field work. The comments of anonymous reviewers and editors A. Coppola and E.O. Frind are gratefully acknowledged.

References

Bouma, J., Jongerius, A., Boersma, O., Jager, A., Schoonderbeek, D., 1977. The function of different types of macropores during saturated flow through four swelling soil horizons. Soil Sci. Soc. Am. J. 41, 945–950.

Bouma, J., Jongerius, A., Schoonderbeek, D., 1979. Calculation of saturated hydraulic conductivity of some pedal clay soils using micromorphometric data. Soil Sci. Soc. Am. J. 43, 261–264.

Bronick, C.J., Lal, R., 2005. Soil structure and management: a review. Geoderma 124, 3–22.

Celis, R., Cox, L., Hermosin, M.C., Cornejo, J., 1997. Sorption of thiazafluron by iron- and humic acid-coated montmorillonite. J. Environ. Qual. 26 (2), 472–479.

Císlerová, M., Šimůnek, J., Vogel, T., 1988. Changes of steady-state infiltration rates in recurrent ponding infiltration experiment. J. Hydrol. 104 (1–4), 1–16.

Coppola, A., et al., 2009. Darcian preferential water flow and solute transport through bimodal porous systems: Experiments and modelling, J. Contam. Hydrol. 104, 74–83 (this issue).

Dousset, S., Thevenot, D., Pot, V., Šimůnek, J., Andreux, F., 2007. Evaluating equilibrium and non-equilibrium transport of bromide and isoproturon in disturbed and undisturbed soil columns. J. Contam. Hydrol. 94, 261–276.

Durner, W., 1994. Hydraulic conductivity estimation for soils with heterogeneous pore structure. Water Resour. Res. 30, 211–233.

Gärdenäs, A., Šimunek, J., Jarvis, N., van Genuchten, M. Th., 2006. Two-dimensional modelling of preferential water flow and pesticide transport from a tile-drained field. J. Hydrol. 329, 647–660.

Gerke, H.H., 2006. Review article. Preferential flow descriptions for structured soils. J. Plant Nutr. Soil Sci. 169, 382–400.

Gerke, H.H., van Genuchten, M.Th., 1993. A dual-porosity model for simulating the preferential movement of water and solutes in structured porous media. Water Resour. Res. 29, 305–319.

German, P.F., Hensel, D., 2006. Poiseuille flow geometry inferred from velocities of wetting front in soils. Vadose Zone J. 5, 867–876.

Jarvis, N., 2007. Review of non-equilibrium water and solute transport in soil macropores: principles, controlling factors and consequences for water quality. Eur. J. Soil Sci. 58, 523–546.

Kočárek, M., Kodešová, R., Kozák, J., Drábek, O., Vacek, O., 2005. Chlorotoluron behaviour in five different soil types. Plant, Soil Environ. 51 (7), 304–309.

Kodešová, R., Kozák, J., Šimůnek, J., Vacek, O., 2005. Single and dual-permeability model of chlorotoluron transport in the soil profile. Plant Soil Environ. 51 (7), 310–315.

Kodešová, R., Kodeš, V., Žigová, A., Šimůnek, J., 2006. Impact of plant roots and soil organisms on soil micromorphology and hydraulic properties. Biologia (Bratisl.) 61 (Supl. 19), S339–S343.

Kodešová, R., Pavlů, L., Kodeš, V., Žigová, A., Nikodem, A., 2007. Impact of spruce forest and grass vegetation cover on soil micromorphology and hydraulic properties of organic matter horizon. Biologia (Bratisl.) 62 (5), 565–568.

Kodešová, R., Kočárek, M., Kodeš, V., Šimůnek, J., Kozák, J., 2008. Impact of soil micromorphological features on water flow and herbicide transport in soils. Vadose Zone J. 7 (2), 798–809 Special Issue "Vadose Zone Modeling".

Köhne, J.M., Köhne, S., Mohanty, B.P., Šimůnek, J., 2005. Inverse mobile–immobile modeling of transport during transient flow: effect of between-domain transfer and initial content. Vadose Zone J. 3, 1309–1321.

Köhne, J.M., Mohanty, B.P., Šimůnek, J., 2006a. Inverse dual-permeability modeling of preferential water flow in a soil column and implications for field-scale solute transport. Vadose Zone J. 5, 59–76.

Köhne, J.M., Köhne, S., Šimůnek, J., 2006b. Multi-process herbicide transport in structured soil columns: experiments and model analysis. J. Contam. Hydrol. 85 (1–2), 1–32.

Köhne, J.M., Köhne, S., Šimůnek, J., 2009a. A Review of Model Applications for Structured Soils: a) Water Flow and Tracer Transport, J. Contam. Hydrol. 104, 4–35 (this issue).

Köhne, J.M., Köhne, S., Šimůnek, J., 2009b. A Review of Model Applications for Structured Soils: b) Pesticide Transport, J. Contam. Hydrol. 104, 36–60 (this issue).

Larsbo, M., Jarvis, N., 2003. MACRO 5.0. A model of water and solute transport in macroporous soil. Technical description. Swedish Univ. of Agricult. Sci., Dept. of Soil Sci., Uppsala, Swedem, Emergo, 6. 48 pp.

Mohanty, B.P., Bowman, R.S., Hendrickx, J.M.H., van Genuchten, M.Th., 1997. New piecewise-continuous hydraulic functions for modeling preferential flow in an intermittent flood-irrigated field. Water Resour. Res. 33, 2049–2063.

Mualem, Y., 1976. A new model for predicting the hydraulic conductivity of unsaturated porous media. Water Resour. Res. 12 (3), 513–522.

Nimmo, J.R., Perkins, K.S., 2002. Aggregate stability and size distribution. In: Dane, J.H., Topp, G.C. (Eds.), Methods of Soil Analysis, Part 4 — Physical Methods. Soil Science Society of America, Inc., Madison, USA, pp. 317–328.

Othmer, H., Diekkrüger, B., Kutílek, M., 1991. Bimodal porosity and unsaturated hydraulic conductivity. Soil Sci. 152 (3), 139–150.

Author's personal copy

Pagliai, M., La Marca, M., Lucamante, G., 1983. Micromorphometric and micromorphological investigations of a clay loam soil in viticulture under zero and conventional tillage. J. Soil Sci. 34, 391–403.
Pagliai, M., Marsili, A., Servadio, P., Vignozzi, N., Pellegrini, S., 2003. Changes in some physical properties of clay soil in central Italy following the passage of rubber tracked and wheeled tractors of medium power. Soil Tillage Res. 73, 119–129.
Pagliai, M., Vignozzi, N., Pellegrini, S., 2004. Soil structure and the effect of management practices. Soil Tillage Res. 79, 131–143.
Pot, V., Šimůnek, J., Benoit, P., Coquet, Y., Yra, A., Martinez Cordun, M.-J., 2005. Impact of rainfall intensity on the transport of two herbicides in undisturbed grassed filter strip soil cores. J. Contam. Hydrol. 81 (1–4), 63–88.
Servadio, P., Marsili, A., Vignozzi, N., Pellegrini, S., Pagliai, M., 2005. Effect on some qualities in central Italy following the passage of four wheel drive tractor fitted with single and dual tires. Soil Tillage Res. 84 (1), 87–100.
Šimůnek, J., Jarvis, N.J., van Genuchten, M. Th., Gärdenäs, A., 2003. Review and comparison of models for describing non-equilibrium and preferential flow and transport in the vadose zone. J. Hydrol. 272, 14–35.
Šimůnek, J., Šejna, M., Saito, H., Sakai, M., van Genuchten, M.Th., 2008a. The HYDRUS-1D Software Package for Simulating the Movement of Water, Heat, and Multiple Solutes in Variably Saturated Media, Version 4.0, HYDRUS Software Series 3, Department of Environmental Sciences, University of California Riverside, Riverside, California, USA, pp. 315.
Šimůnek, J., van Genuchten, M. Th., 2008b. Modeling nonequilibrium flow and transport with HYDRUS. Vadose Zone J. 7 (2), 782–797 Special Issue "Vadose Zone Modeling".
Six, J., Elliott, E.T., Paustian, K., Doran, J.W., 1998. Aggregation and soil organic matter accumulation in cultivated and native grassland soils. Soil Sci. Soc. Am. J. 62, 1367–1377.
Six, J., Feller, C., Denef, K., Ogle, S.M., 2002. Soil organic matter, biota and aggregation in temperate and tropical soils — effect of no-tillage. Agronomie 22, 755–775.
UMS GmbH, Munich, 2005. T5 Miniature Pressure Transducer Tensiometer, User Manual version 1.8, Munich.
van Genuchten, M. Th., 1980. A closed-form equation for predicting the hydraulic conductivity of unsaturated soils. Soil Sci. Soc. Am. J. 44, 892–898.
van Genuchten, M.T., Wagenet, R.J., 1989. Two-site/two-region models for pesticide transport and degradation: theoretical development and analytical solutions. Soil Sci. Soc. Am. J. 53, 1303–1310.
Watson, K.W., Luxmoore, R.J., 1986. Estimating macroporosity in a forest watershed by use of a tension infiltrometer. Soil Sci. Soc. Am. J. 50 (3), 578–582.